THE JOURNAL OF PHYSICAL CHEMISTRY C

C: Plasmonics; Optical, Magnetic, and Hybrid Materials

Efficient UV Luminescence from Organic-Based Tamm Plasmon Structures Emitting in the Strong Coupling Regime

Konstantin M. Morozov, Konstantin A. Ivanov, Alexey V. Belonovski, Elizaveta I. Girshova, Daniel De Sa Pereira, Christopher Menelaou, Piotr Henryk Pander, Larissa Gomes Franca, Andrew P. Monkman, Galia Pozina, Daniil A. Livshits, Nikita V. Selenin, and Mikhail A. Kaliteevski

J. Phys. Chem. C, **Just Accepted Manuscript** • DOI: 10.1021/acs.jpcc.0c05091 • Publication Date (Web): 09 Sep 2020

Efficient UV Luminescence from Organic-Based Tamm Plasmon Structures Emitting in the Strong Coupling Regime

*Konstantin M. Morozov[1, *], Konstantin A. Ivanov[2], Alexey V. Belonovski[1], Elizaveta I. Girshova[1], Daniel de Sa Pereira[3], Christopher Menelaou[3], Piotr Pander[3], Larissa G. França[3], Andrew P. Monkman[3], Galia Pozina[4], Daniil A. Livshits[5], Nikita V. Selenin[5] and Mikhail A. Kaliteevski[1, 2, *]*

[1] Alferov University, 8/3 Khlopina Str., St. Petersburg, 194021, Russia

[2] ITMO University, 49 Kronverksky Pr., St. Petersburg, 197101, Russia

[3] Physics Department, Durham University, Durham, DH1 3LE, UK

[4] Department of Physics, Chemistry and Biology, Linköping University, 58183, Linköping, Sweden

[5] Innolume GmbH, Konrad-Adenauer-Allee 11, 44263, Dortmund, Germany

* The correspondence should be sent to morzconst@gmail.com and m.kaliteevski@mail.ru

Abstract

Excitons in organic semiconductors possessing a large oscillator strength demonstrate strong coupling with cavity modes at room temperature. A large Stokes shift in some organic semiconductors enriches and complicates the picture of the emission in strongly coupled systems of organic excitons and light. Here we demonstrate strong coupling of excitons in 4,4-Bis(N-carbazolyl)-1,1-biphenyl (CBP) and Tamm plasmons in the UV band, accompanied by a bright emission from the structure. Reflection measurements demonstrate the pronounced formation of the lower and upper polariton modes with

Rabi splitting of the magnitude of 0.3 eV, and the emission peak experiences a substantial red shift with respect to the lower polariton mode. Both radiative and non-radiative decay rates in the Tamm plasmon CBP structure are increased with respect to a bare CBP. Such peculiar behavior is attributed to the simultaneous manifestation of strong coupling and weak coupling of the CBP molecule emitters to the Tamm plasmons.

Introduction

Progress in material synthesis allows the observation of light-matter coupling in specially designed photonic crystals, periodic structures, metamaterials and other nanostructures. Strong coupling between excitons and optical cavity modes in inorganic microcavities and organic material system[1-6] have opened a new chapter in the exploration of light - matter interaction with potential in many future applications such as polariton lasers,[7] polariton light-emitting diodes[8] and polariton switches,[9] which can be an essential contribution to the development of different aspects of our society from sustainable energy systems to telecommunication technology.

Importantly, the emission and absorption properties of optically active materials can be strongly modified in the media with a spatially inhomogeneous dielectric function. In the periodic media such as photonic crystals, suppression of spontaneous emission occurs when the frequency of the optical transition corresponds to the photonic bandgap (PBG)[10-12] while at the edges of the PBG the light-matter interaction is enhanced.[13-15] In the case when an emitter is placed in a cavity and when the frequency of emission corresponds to the cavity mode, a new set of phenomena appears. Namely, depending on the strength of the light-matter interaction and the decay rates, the system of a coupled emitter and cavity mode could interact in the weak or strong coupling regime. In the weak coupling regime, the probability of spontaneous emission increases manifesting the Purcell effect[16-18] which can be utilized in vertical-cavity lasers.[19-21] In the strong coupling regime, the emitted photon is reabsorbed, then reemitted and reabsorbed again and again, and this process leads to the mixing of the cavity and emitter modes and the formation of upper and lower polaritons separated by so-called Rabi splitting,[1,22,23] as illustrated in Figure 1a. In connection to this phenomenon, organic semiconductors attract much attention because the exciton

oscillator strength in such materials can be much larger than in inorganic semiconductors leading, in turn, to a huge Rabi splitting as high as few hundreds meV[24-26] meaning that a strong coupling regime can be easily achieved even at room temperature. For example, J-aggregates characterizing by a sharp absorption peak and a small Stokes shift have been widely used for studies of strongly coupled two-level systems in organics.[27-29]

The situation when the frequencies of emission and absorption are almost the same, is typical for atoms and excitons in inorganic semiconductors. However, in most of the organic molecules, a conformational rearrangement and energy relaxation follow the absorption of light, which can lead to a reduction of the photon energy and a large Stokes shift between the absorption and the emission peaks.[30-34] The studies of emission, transmission and reflection properties of the materials with a large Stokes shift indicate that the polariton modes corresponding to a strong coupling regime are formed by the cavity mode and exciton absorption resonance.[24] At the same time, it is unclear how the strong coupling between the cavity mode and the “absorbing exciton” can influence the emission properties of the system of the cavity with the material where

the emission and absorption peaks are shifted with respect to each other (see Figure 1b). Furthermore, the picture of light matter-coupling in organic materials becomes more reach and complicated, since the spectrum of organic molecules is characterized by few hundreds of vibrational modes [35-38] leading to various phenomena originated from Franck-Condon effect. [39-42]

Thus, this paper is aimed at the investigation of the luminescence properties in strongly coupled systems with an organic emitter where the value of the Stokes shift is comparable to the splitting of the modes in specially designed Tamm plasmon (TP) structures.[43,44] Additionally, we have studied the properties of TPs in the ultraviolet (UV) band [45,46] when the absorption effects in the metal could substantially increase the decay of polariton modes.

Experimental section

The CBP/TP structure under the study was fabricated according to the following procedure. First, a 5 pair distributed Bragg reflector (DBR) was deposited on a SiO_2

substrate using ion assisted ion beam spattering. The thicknesses of the DBR layers were chosen to be 43 nm for the Ta_2O_5 layer and 66 nm for the SiO_2 layer, to provide a photonic bandgap centred at 3.17 eV, which corresponds to the CBP emission band. Then, using a Kurt J. Lesker Spectros II system (organic and metal thin film deposition system capable of reaching vacuum levels as low as 1 $\times 10^{-6}$ mbar) 26 nm CBP and 50 nm silver layers were deposited on top of the DBR. Three TP/CBP samples with identical parameters were fabricated in three different evaporation procedures on the same DBR substrate for the reliability of the results. For comparison of emission properties, a CBP layer of thickness 50 nm was grown on Al_2O_3 substrate. To achieve the required thicknesses of the CBP and silver, several calibration deposits of both materials and thickness measurements (using J. A. Woollam VASE Ellipsometer) were performed. Also, a set of Ag thin films (40nm, 50nm, 60nm) were deposited on the quartz substrate for investigation of the silver part of the Tamm plasmon cavity properties (see Supporting Information, Section S1).

Measurement of the angle-resolved reflectivity spectra of the TP/CBP structure (from 20 degrees to 90 degrees with step 5 degrees; Number of revolutions 10) for the TE-

polarization was performed by the J. A. Woollam VASE Ellipsometer system. As well as measurements of the thin films thickness and their optical constants (n and k values). The fit of the experimentally measured thickness and the optical constants were carried out by the WVASE software.

The photoluminescence (PL) spectra of the bare CBP and the set of TP structures were measured using a Jobin-Yvon Horiba Fluorolog FL3-22 spectrometer (the neat CBP was excited at 4.27 eV) at room temperature and atmospheric pressure. Jobin-Yvon Horiba Fluorolog FL3-22 equipped with 450W Xenon lamp light source and two double-grating spectrometer schemes. The neat CBP layer shows a wide emission band in the frequency interval from 2.8 eV to 3.3 eV, and the emission spectrum almost does not depend on the emission angle. Note, that luminescence properties of various samples of CBP could differ for number reasons described in [31] due to chemical transformation in condensed CBP, leading to violation of exponential law of luminescence decay.[47] The TP/CBP structures were excited through the metallic layer with the different excitation energy. Samples were placed on the rotational holder and the emission from the sample was collected at various angles.

Decay dynamics of the excited states of the CBP coupled with a Tamm plasmon state and in free space (reference neat CBP sample) were measured using time-correlated single-photon counting (TCSPC) at room temperature and in 1×10^{-4} mbar vacuum. The structure was excited through the silver layer at 4.73eV energy (the third harmonic of Coherent Mira 900-F Ti: Sapphire oscillator tuned to 786 nm central wavelength) with a 76 MHz repetition rate. Samples were excited at a 45 degrees angle to the substrate normal. Emission from the sample was collected also at a 45 degrees angle to the substrate normal at various energies (from 3.22 eV to 3.44 eV).

Results and discussion

For the investigation of the properties of interaction of the UV TP with the material with a large Stocks shift, we fabricated TP structure with the layer of organic material 4,4-Bis(N-carbazolyl)-1,1-biphenyl (CBP), see Figure 1c. CBP is one of the most popular materials used as the hosts for red, yellow, green, as well as blue emitters in OLEDs due to its relatively large bandgap and ambipolarity.[48,49] Also, CBP is a

perspective material for advanced plasmonic devices since the interface between CBP and Ag supports the surface plasmon with a frequency corresponding to the emission band of CBP.[50]

Refractive index of the neat CBP layer obtained by ellipsometry measurements are demonstrated in Figure 1d. There is a well-pronounced peak of an imaginary part of the refractive index *n*, centred at an energy of 3.5 eV followed by an absorption band at the higher photon energies.

An absorption peak is an evidence of an exciton in the CBP, and in the vicinity of the exciton resonance dielectric function of CBP can be written as

$$\varepsilon_{CBP} = \varepsilon_b + \frac{\omega_{LT}}{\omega_{exc} - \omega - i\gamma_{exc}} \quad (1)$$

with background dielectric constant $\varepsilon_b = 3.9$, exciton resonance frequency ω_{exc}= 3.5 eV, oscillator strength ω_{LT} = 26 meV and the exciton non-radiative damping γ_{exc} = 0.15 eV. CPB photoluminescence (PL) spectrum is shown in Figure 1d, demonstrating the wide emission band with a maximum at 3.17 eV, thus the value of the Stokes shift for CBP is about 350 meV.

To arrange strong coupling of the CBP exciton to the electromagnetic field, the Tamm plasmon (TP) structure with the layer of CBP was fabricated. Figure 2a shows the scheme of the structure under study, which consists of 5 –period SiO_2/ Ta_2O_5 Bragg reflector (BR), a layer of CBP with the thickness 26 nm and 50 nm thick top mirror made from silver. Scanning electron microscope (SEM) image of the fabricated structure demonstrated in Figure 2b.

Reflectivity spectra of the Bragg reflector and silver layer (Figure 1d were calculated using a transfer-matrix method (TMM) with optical parameters of Ta_2O_5, SiO_2 and Ag layers from [51,52]. Comparison of the calculated spectra of the reflection coefficient with experimental spectra of the silver mirror used in our experiments are provided in Section S1 of the Supporting Information. It can be seen that the Bragg reflector provides a reflection coefficient of about 70% for the frequency region from 2.9 eV to 3.6 eV. The reflection coefficient of the silver mirror reduces monotonically from 90% at 2.5 eV to 10% at 4eV.

Interaction of the TP and the CBP exciton leads to the formation of the two polariton modes: upper polariton (UP) and lower polariton (LP) with energies defined by equation

$$\omega_{UP,\ LP}(\theta) = \frac{\omega_{exc} + \omega_{TP}(\theta)}{2} - \frac{i(\gamma_{exc} + \gamma_{TP})}{2} \pm \frac{\Omega(\theta)}{2} \quad (2)$$

where $\omega_{\mathrm{TP}}(\theta)$ and γ_{TP} are the Tamm plasmon frequency and non-radiative decay, respectively and $\Omega(\theta)$ is the Rabi splitting

$$\Omega(\theta) = 2 \cdot \sqrt{V^2 + \frac{1}{4}(\omega_{exc} - \omega_{TP}(\theta) - i(\gamma_{exc} - \gamma_{TP}))^2} \quad (3)$$

The design of the structure was chosen to provide an energy of the TP equal to 3.2 eV at normal incidence, which is 0.3 eV below the energy of the exciton, the decay of bare TP $\gamma_{TP} =$ 0.17 eV. Figure 3a shows a calculated and measured pattern of the reflection coefficient. It can be seen that there are two dips, associated with UP and LP modes. The UP mode is less pronounced due to the reduction of the reflection coefficient of the silver layer at the photon energies above 3.5 eV (see Figure 1d). The UP and LP demonstrate anti-crossing behavior, indicating realization of the strong coupling regime. For the incidence angle of 45 degrees the energies of the uncoupled TP and exciton in CBP become equal, splitting of the UP and LP at the anti-crossing point of 0.3 eV, thus parameter V = 0.15 eV.

Figure 3b show the measured and calculated reflection spectra for incidence angle of 25, 45 and 60 degrees. The green circles in Figure 3a shows the result of the fitting of dips in the reflectivity spectra with Lorentz line shapes. It can be seen that despite the reduction of reflectivity of the silver layer in the UV band, strong coupling of the exciton and Tamm plasmon can be realized. At the same time, for UP branch when the reflectivity of silver layer is reduced while absorption of the layer is increased in respect to LP light-matter coupling becomes much weaker, which manifests itself as an increased width and reduced depth of spectral width of the feature, corresponding to UP, as shown in figure 3b.

Now, it is interesting to investigate the luminescence properties of the TP CBP structure. Figure 4a demonstrates the calculated pattern of the modal Purcell factor $F_m(\theta)$[53] (the ratio of the spontaneous emission probability per interval of energy per interval of solid angle for the emitter placed into the structure and emitter in the free space, details in Section S2 of the Supporting Information) for the emitter placed in the centre of CBP layer. Purcell factor F_p in its usual sense, defined as the ratio of spontaneous emission rate for emitter placed in the cavity and free space is the integral

of modal Purcell factor $F_m(\theta)$ over a solid angle. It can be seen, that the spectral positions of the LP and UP branches, calculated using expression (2) corresponds to the areas of the increased modal Purcell factor. Two other regions of increased modal Purcell factor distribution in Figure 4 with energies 2.9 eV and 3.7 eV near the PBG edges (dashed blue curves) correspond to the DBR's localized edge states. An increase of the modal Purcell factor is defined by the local magnitude of the electric field of the mode.

The product of the modal Purcell factor and occupancy of the state define the dependence of emission intensity on the frequency and angle of emission. In the case of TP structures with quantum dots [53] (where the capture time of non equilibrium electrons and holes on quantum dots is very small and relaxation of electrons is negligible) emission spectrum of the structure is just the product of the emission spectrum of bare quantum dots to the modal Purcell factor. In organic systems, there are many channels of exciton relaxation processes [54-56] and the resulting emission spectrum depends on the relaxation processes and consequently on the excitation conditions. It can be seen that $F_m(\theta)$ is substantially increased near the bottom of the

LP branch and is decreasing with an increase of angle θ. Reduction of F_m with increasing θ is explained by the change of the electric field profile of the eigenmode. Figures 4 b, c, d demonstrates the profile of the quantity $\tilde{I} = |\tilde{\epsilon}^{(1)}|^2 + |\tilde{\epsilon}^{(2)}|^2$, which is proportional to the electric field squared of the eigenmode in the LP branch, for different angles θ: 0 degrees (4b); 45 degrees (4c); and 85 degrees (4d). When $\theta = 0$ degrees, the electric field is localized on the CBP layer, for $\theta = 45$ degrees the field is less localized, and for $\theta = 85$ degrees the field is localized on the side of the BR, opposite to the layer of CBP.

Figure 5 shows the pattern of steady-state room temperature PL, taken under excitation of the TP structure with radiation of different photon energy: 4.76 eV (Figure 5a), 4.27 eV (Figure 5b) and 3.75 eV (Figure 5c). The excitation density was the same in all 3 cases. It can be seen that for all three excitation photon energies the PL occurs near the LP branch, but the PL peak energy is shifted down by 50 – 70 meV with respect to the LP branch for the angles $\theta > 30$ degrees, but on other hand it is shifted up in respect to the peak of the bare CBP emission line. It can also be seen, that the PL intensity reduces dramatically with an increasing difference between the photon

energies of excitation and luminescence. The decrease of the PL intensity with increasing of the off-set of excitation can be explained by the existance of multiple channels of the PL quenching in organic materials,[57-59] which occurs faster than the energy relaxation.

Like most of the organic molecules, excited singlet state of CBP has a set of vibronic sublevels (singlet manifold).[35] Exciting high in the singlet manifold results in a rapid internal conversion (IC) and vibrational relaxation (characteristic rate lies in the range of values between 10^{11} – 10^{14} s^{-1}) to excited singlet state S1 and then radiative decay (characteristic fluorescence rate is around 10^{9} s^{-1}). The main non-radiative relaxation mechanism is an intersystem crossing (ISC) from singlets to triplets [60] (characteristic rate usually in the range of values between 10^{9} – 10^{11} s^{-1}). For the carbazoles the latter channel has a high yield.[31,61] Due to the high rates of the ISC PL pattern differs strongly with varying the excitation energy: with increasing of the excitation energy, the probability of the non-radiative migration of the excited singlet increases which leads to lesser PL intensity.

The PL spectra taken at different emission angles θ are shown in Figure 6a. It can be seen the emission lines of the TP CBP structure have different shapes and smaller width in respect to those of the bare CBP, and furthermore its spectral position depends of the emission angles θ.The difference between the position of the LP and the PL photon energy allows to suggest that for the system with a large Stokes shift considered, the mechanism of luminescence is different from the usual polaritonic luminescence from the microcavity operating in the strong coupling regime. Figure 6b shows the product of the modal Purcell factor F_m shown in Figure 4a, and the CBP emission intensity I_{CBP}. For comparison, the position of the PL peaks for the three samples used in this study are shown by circles.

The photoluminescence spectra of strongly coupled exciton and cavity modes can be calculated using the quantum mechanical formalism based on density matrix of the system developed in [62] (see section S3 of Supporting information), and it can be seen, that for LP angular dependence of experimentally observed and calculated spectra are qualitatively similar.

In the system, where the relaxation excited emitter is not pronounced, such product of the modal Purcell factor and the emission spectrum of the bare emitter is nothing but the emission intensity of the structure.[53] Figure 6b shows, that the experimentally measured dependence of the PL peak position coincides with the maximum values of the product $F_m I_{CBP}$, though the experimentally observed pattern of luminescence does not repeat the pattern of the quantity $F_m I_{CBP}$ due to its fast processes of relaxation and non-radiative quenching of the emission. Coincidence of the peak positions in the experimentally observed spectra and the ridge of the quantity $F_m I_{CBP}$ allows to conclude that the emission pattern is formed in the following way:

- first, interaction of the absorbing exciton in the CBP and the TP in the strong coupling regime modifies the local density of photonic state, providing an increase of the spontaneous emission rate in the areas near the polariton branches;
- then, the spontaneous emission of the bare CBP is modified via Purcell effect in the weak coupling regime.

Existence of the Purcell effect should be accompanied by the modification of the spontaneous emission rate described by the Purcell coefficient F_P. Figure 6c shows the calculated dependence of the Purcell coefficient, demonstrating the peak near the photon energy of 3.2 eV within the emission band of the CBP.

In the experiments, the Purcell effect manifests itself as a modification of the radiative decay time. For the study of the radiative decay and the non-radiative quenching processes at room temperature, time-resolved PL measurements for a set of emission energies at a fixed angle (45 degrees) were carried out by means of the time-correlated single-photon counting (TCSPC) method. For comparison, time-resolved spectra of the bare CBP layer sample were measured.

Figure 7a shows the temporal dependence of the PL intensity for the photon energy of 3.35 eV after pulsed excitation. It can be seen, that the dependence demonstrates bi-exponential decay [50] for the time interval of 1 ns, there is “fast” decay, characterized by decay time $\tau_{CBP}^{(1)}$= 0.24 ns, and then, PL experiences “slow” decay, characterized by $\tau_{CBP}^{(2)}$ =1.1 ns. The luminescence of the TP CBP structure (see Figure 7b) also demonstrates

bi-exponential decay, characterized by the "fast" part with decay time $\tau_{LP}^{(1)}$ = 0.12ns, and the "slow" part with $\tau_{LP}^{(2)}$.

Figure 6c along with the calculated Purcell coefficient F_P shows the ratios $\tau_{CBP}^{(1)}/\tau_{LP}^{(1)}$ (blue circles) and $\tau_{CBP}^{(2)}/\tau_{LP}^{(2)}$ (red circles) corresponding to "fast" and "slow" decays. In the absence of additional non-radiative quenching of luminescence, caused by influence of the metallic layer, these ratios should be equal to the Purcell coefficient. As can be seen, the ratios $\tau_{CBP}^{(1)}/\tau_{LP}^{(1)}$ and $\tau_{CBP}^{(2)}/\tau_{LP}^{(2)}$ are similar for "fast" and "slow" cases. It's clear that the measured lifetime ratios for various energies mimic the dependence of the calculated Purcell factor F_P corresponded to the LP branch with an upward shift of the value of 1.2 approximately. The difference between the measured ratios of decay time and the calculated Purcell factor value is explained by quenching of the organic emitter located near the silver layer.[50]

Conclusions

In conclusion, we have studied the luminescent properties of the organic material 4,4-Bis(N-carbazolyl)-1,1-biphenyl (CBP) with high values of the Stokes shift, emitting in the near-UV spectral region strongly coupled to the Tamm plasmon (TP) cavity mode. Reflectivity, steady-state and time-resolved PL measurements along with the calculation of dispersion of the polariton modes, the Purcell coefficient, reflectivity and luminescence spectra were carried out. It was demonstrated by reflectivity measurements, that there is strong coupling between the TP and the “absorbing” exciton in the CBP. Luminescence experiences 50 meV red shift with respect to the lower polariton branch.

It was proposed that the luminesce pattern in the structure is formed in the following way: strong coupling of the Tamm plasmon and absorbing exciton in the CBP modifies the probability of the spontaneous emission rate near the polariton branches, then the molecule of CBP absorbs light and experiences conformational rearrangement and energy relaxation, and then the molecule emits light with modified spontaneous emission rate.

Analysis of the calculated Purcell coefficient and measured luminescence decay time shows that there is intensive quenching of the luminescence near the interface between CBP and silver.

Acknowledgments

The work has been supported by Russian Science Foundation 16-12-10503, the Swedish Research Council (Grant 2019-05154), Swedish Energy Agency (Grant 46563-1).

Supporting Information

Section S1: Optical properties of thin silver films.; Section S2: Modal Purcell factor calculation.; Section S3: Luminescence spectra calculation and comparison with the experimental PL data.

References

(1) Weisbuch, C.; Nishioka, M.; Ishikawa, A.; Arakawa, Y. Observation of the Coupled Exciton-Photon Mode Splitting in a Semiconductor Quantum Microcavity. *Phys. Rev. Lett.* **1992**, *69* (23), 3314–3317.

(2) Lidzey, D. G.; Bradley, D. D. C.; Skolnick, M. S.; Virgili, T.; Walker, S.; Whittaker, D. M. Strong Exciton–photon Coupling in an Organic Semiconductor Microcavity. *Nature* **1998**, *395* (6697), 53–55.

(3) Holmes, R. J.; Forrest, S. R. Strong Exciton-Photon Coupling and Exciton Hybridization in a Thermally Evaporated Polycrystalline Film of an Organic Small Molecule. *Phys. Rev. Lett.* **2004**, *93* (18), 186404.

(4) Kéna-Cohen, S.; Forrest, S. R. Room-Temperature Polariton Lasing in an Organic Single-Crystal Microcavity. *Nat. Photonics* **2010**, *4* (6), 371–375.

(5) Somaschi, N.; Mouchliadis, L.; Coles, D.; Perakis, I. E.; Lidzey, D. G.; Lagoudakis, P. G.; Savvidis, P. G. Ultrafast Polariton Population Build-up Mediated by Molecular Phonons in Organic Microcavities. *Appl. Phys. Lett.* **2011**, *99* (14), 143303.

(6) Paschos, G. G.; Somaschi, N.; Tsintzos, S. I.; Coles, D.; Bricks, J. L.; Hatzopoulos, Z.; Lidzey, D. G.; Lagoudakis, P. G.; Savvidis, P. G. Hybrid Organic-Inorganic Polariton Laser. *Sci. Rep.* **2017**, *7*, 11377.

(7) Bhattacharya, P.; Frost, T.; Deshpande, S.; Baten, M. Z.; Hazari, A.; Das, A. Room Temperature Electrically Injected Polariton Laser. *Phys. Rev. Lett.* **2014**, *112*, 236802.

(8) Tsintzos, S. I.; Pelekanos, N. T.; Konstantinidis, G.; Hatzopoulos, Z.; Savvidis, P. G. A GaAs Polariton Light-Emitting Diode Operating near Room Temperature. *Nature* **2008**, *453* (7193), 372–375.

(9) Gao, T.; Eldridge, P. S.; Liew, T. C. H.; Tsintzos, S. I.; Stavrinidis, G.; Deligeorgis, G.; Hatzopoulos, Z.; Savvidis, P. G. Polariton Condensate Transistor Switch. *Phys. Rev. B* **2012**, *85*, 235102.

(10) Yablonovitch, E. Inhibited Spontaneous Emission in Solid-State Physics and Electronics. *Phys. Rev. Lett.* **1987**, *58* (20), 2059–2062.

(11) Bykov, V. P. Spontaneous emission in a periodic structure. *Sov. Phys. JETP* **1972,** *35* (2), 269–273.

(12) Krauss, T. F.; Rue, R. M. D. L.; Brand, S. Two-Dimensional Photonic-Bandgap Structures Operating at near-Infrared Wavelengths. *Nature* **1996**, *383* (6602), 699–702.

(13) Kogelnik, H.; Shank, C. V. Coupled-Wave Theory of Distributed Feedback Lasers. *J. Appl. Phys.* **1972**, *43* (5), 2327–2335.

(14) Askitopoulos, A.; Mouchliadis, L.; Iorsh, I.; Christmann, G.; Baumberg, J. J.; Kaliteevski, M. A.; Hatzopoulos, Z.; Savvidis, P. G. Bragg Polaritons: Strong Coupling and Amplification in an Unfolded Microcavity. *Phys. Rev. Lett.* **2011**, *106* (7), 076401.

(15) Kaliteevski, M. A.; Beggs, D. M.; Brand, S.; Abram, R. A.; Nikolaev, V. V. Statistics of the Eigenmodes and Optical Properties of One-Dimensional Disordered Photonic Crystals. *Phys. Rev. E* **2006**, *73* (5), 056616.

(16) Purcell, E. M. Spontaneous emission probabilities at radio frequencies. *Phys. Rev.* **1946**, *69*, 681.

(17) Liu, F.; Brash, A. J.; O'Hara, J.; Martins, L. M. P. P.; Phillips, C. L.; Coles, R. J.; Royall, B.; Clarke, E.; Bentham, C.; Prtljaga, N.; et al. High Purcell Factor Generation of Indistinguishable on-Chip Single Photons. *Nat. Nanotechnol.* **2018**, *13* (9), 835–840.

(18) Muljarov, E. A.; Langbein, W. Exact Mode Volume and Purcell Factor of Open Optical Systems. *Phys. Rev. B* **2016**, *94* (23), 235438.

(19) Iga, K.; Koyama, F.; Kinoshita, S. Surface Emitting Semiconductor Lasers. *IEEE J. Quantum Electron.* **1988**, *24* (9), 1845–1855.

(20) Kako, S.; Someya, T.; Arakawa, Y. Observation of Enhanced Spontaneous Emission Coupling Factor in Nitride-Based Vertical-Cavity Surface-Emitting Laser. *Appl. Phys. Lett.* **2002**, *80* (5), 722–724.

(21) Khurgin, J. B.; Sun, G. Comparative Analysis of Spasers, Vertical-Cavity Surface-Emitting Lasers and Surface-Plasmon-Emitting Diodes. *Nat. Photonics* **2014**, *8* (6), 468–473.

(22) Deng, H.; Haug, H.; Yamamoto, Y. Exciton-Polariton Bose-Einstein Condensation. *Rev. Mod. Phys.* **2010**, *82* (2), 1489–1537.

(23) Houdré, R.; Weisbuch, C.; Stanley, R. P.; Oesterle, U.; Pellandini, P.; Ilegems, M. Measurement of Cavity-Polariton Dispersion Curve from Angle-Resolved Photoluminescence Experiments. *Phys. Rev. Lett.* **1994**, *73* (15), 2043–2046.

(24) Ballarini, D.; De Giorgi, M.; Gambino, S.; Lerario, G.; Mazzeo, M.; Genco, A.; Accorsi, G.; Giansante, C.; Colella, S.; D'Agostino, S.; et al. Polariton-Induced Enhanced Emission from an Organic Dye under the Strong Coupling Regime. *Adv. Opt. Mater.* **2014**, *2* (11), 1076–1081.

(25) Daskalakis, K. S.; Maier, S. A.; Murray, R.; Kéna-Cohen, S. Nonlinear Interactions in an Organic Polariton Condensate. *Nat. Mater.* **2014**, *13* (3), 271–278.

(26) Kéna-Cohen, S.; Maier, S. A.; Bradley, D. D. C. Ultrastrongly Coupled Exciton-Polaritons in Metal-Clad Organic Semiconductor Microcavities. *Adv. Opt. Mater.* **2013**, *1* (11), 827–833.

(27) Lidzey, D. G.; Bradley, D. D. C.; Virgili, T.; Armitage, A.; Skolnick, M. S.; Walker, S. Room Temperature Polariton Emission from Strongly Coupled Organic Semiconductor Microcavities. *Phys. Rev. Lett.* **1999**, *82* (16), 3316–3319.

(28) Lidzey, D. G.; Bradley, D. D. C.; Armitage, A.; Walker, S.; Skolnick, M. S. Photon-Mediated Hybridization of Frenkel Excitons in Organic Semiconductor Microcavities. *Science* **2000**, *288* (5471), 1620–1623.

(29) Lidzey, D. G.; Fox, A. M.; Rahn, M. D.; Skolnick, M. S.; Agranovich, V. M.; Walker, S. Experimental Study of Light Emission from Strongly Coupled Organic Semiconductor Microcavities Following Nonresonant Laser Excitation. *Phys. Rev. B* **2002**, *65* (19), 195312.

(30) Brückner, R.; Zakhidov, A. A.; Scholz, R.; Sudzius, M.; Hintschich, S. I.; Fröb, H.; Lyssenko, V. G.; Leo, K. Phase-Locked Coherent Modes in a Patterned Metal–organic Microcavity. *Nat. Photonics* **2012**, *6* (5), 322–326.

(31) Jankus, V.; Winscom, C.; Monkman, A. P. The Photophysics of Singlet, Triplet, and Degradation Trap States in 4,4-N,N′-Dicarbazolyl-1,1′-Biphenyl. *J. Chem. Phys.* **2009**, *130* (7), 74501.

(32) Peng, X.; Song, F.; Lu, E.; Wang, Y.; Zhou, W.; Fan, J.; Gao, Y. Heptamethine Cyanine Dyes with a Large Stokes Shift and Strong Fluorescence: A Paradigm for

Excited-State Intramolecular Charge Transfer. *J. Am. Chem. Soc.* **2005**, *127* (12), 4170– 71.

(33) Sednev, M. V.; Belov, V. N.; Hell, S. W. Fluorescent Dyes with Large Stokes Shifts for Super-Resolution Optical Microscopy of Biological Objects: A Review. *Methods Appl. Fluoresc.* **2015**, *3* (4), 42004.

(34) Coles, D. M.; Michetti, P.; Clark, C.; Tsoi, W. C.; Adawi, A. M.; Kim, J.-S.; Lidzey, D. G. Vibrationally Assisted Polariton-Relaxation Processes in Strongly Coupled Organic-Semiconductor Microcavities. *Adv. Funct. Mater.* **2011**, *21* (19), 3691–3696.

(35) George, J.; Wang, S.; Chervy, T.; Canaguier-Durand, A.; Schaeffer, G.; Lehn, J.-M.; Hutchison, J. A.; Genet, C.; Ebbesen, T. W. Ultra-Strong Coupling of Molecular Materials: Spectroscopy and Dynamics. *Faraday Discuss.* **2015**, *178*, 281–294.

(36) Wang, S.; Chervy, T.; George, J.; Hutchison, J. A.; Genet, C.; Ebbesen, T. W. Quantum Yield of Polariton Emission from Hybrid Light-Matter States. *J. Phys. Chem. Lett.* **2014**, *5* (8), 1433–1439.

(37) Ćwik, J. A.; Reja, S.; Littlewood, P. B.; Keeling, J. Polariton Condensation with Saturable Molecules Dressed by Vibrational Modes. *EPL* **2014**, *105* (4), 47009.

(38) Canaguier-Durand, A.; Genet, C.; Lambrecht, A.; Ebbesen, T. W.; Reynaud, S. Non-Markovian Polariton Dynamics in Organic Strong Coupling. *Eur. Phys. J. D* **2015**, *69* (1), 24.

(39) Lax, M. The Franck-Condon Principle and Its Application to Crystals. *The Journal of Chemical Physics* **1952**, *20* (11), 1752–1760.

(40) Bayliss, N. S.; McRae, E. G. Solvent Effects in Organic Spectra: Dipole Forces and the Franck–Condon Principle. *J. Phys. Chem.* **1954**, *58* (11), 1002–1006.

(41) Wilhelm, P.; Vogelsang, J.; Schönfelder, N.; Höger, S.; Lupton, J. M. Anomalous Linear Dichroism in Bent Chromophores of π -Conjugated Polymers: Departure from the Franck-Condon Principle. *Phys. Rev. Lett.* **2019**, *122* (5), 057402.

(42) Smith, W. L. The Franck–Condon Principle and the Sudden Approximation. *Spectrochimica Acta Part A: Molecular and Biomolecular Spectroscopy* **2009**, *72* (1), 222–227.

(43) Sasin, M. E.; Seisyan, R. P.; Kalitteevski, M. A.; Brand, S.; Abram, R. A.; Chamberlain, J. M.; Egorov, A. Y.; Vasil'ev, A. P.; Mikhrin, V. S.; Kavokin, A. V. Tamm Plasmon Polaritons: Slow and Spatially Compact Light. *Appl. Phys. Lett.* **2008**, *92* (25), 251112.

(44) Goto, T.; Dorofeenko, A. V.; Merzlikin, A. M.; Baryshev, A. V.; Vinogradov, A. P.; Inoue, M.; Lisyansky, A. A.; Granovsky, A. B. Optical Tamm States in One-Dimensional Magnetophotonic Structures. *Phys. Rev. Lett.* **2008**, *101* (11), 113902.

(45) Yang, Y.; Callahan, J. M.; Kim, T.-H.; Brown, A. S.; Everitt, H. O. Ultraviolet Nanoplasmonics: A Demonstration of Surface-Enhanced Raman Spectroscopy, Fluorescence, and Photodegradation Using Gallium Nanoparticles. *Nano Lett.* **2013**, *13* (6), 2837–2841.

(46) Gutiérrez, Y.; Ortiz, D.; Saiz, J.; González, F.; Everitt, H.; Moreno, F. The UV Plasmonic Behavior of Distorted Rhodium Nanocubes. *Nanomaterials* **2017**, *7* (12), 425.

(47) Rothe, C.; Hintschich, S. I.; Monkman, A. P. Violation of the Exponential-Decay Law at Long Times. *Phys. Rev. Lett.* **2006**, *96* (16).

(48) Adamovich, V.; Brooks, J.; Tamayo, A.; Alexander, A. M.; Djurovich, P. I.; D'Andrade, B. W.; Adachi, C.; Forrest, S. R.; Thompson, M. E. High Efficiency Single Dopant White Electrophosphorescent Light Emitting diodes. *New J. Chem.* **2002**, *26* (9), 1171–1178.

(49) Sun, Y.; Giebink, N. C.; Kanno, H.; Ma, B.; Thompson, M. E.; Forrest, S. R. Management of Singlet and Triplet Excitons for Efficient White Organic Light-Emitting Devices. *Nature* **2006**, *440* (7086), 908–912.

(50) Morozov, K. M.; Ivanov, K. A.; de Sa Pereira, D.; Menelaou, C.; Monkman, A. P.; Pozina, G.; Kaliteevski, M. A. Revising of the Purcell Effect in Periodic Metal-Dielectric Structures: The Role of Absorption. *Sci. Rep.* **2019**, *9* (1), 9604.

(51) Rodríguez-de Marcos, L. V.; Larruquert, J. I.; Méndez, J. A.; Aznárez, J. A. Self-Consistent Optical Constants of SiO_2 and Ta_2O_5 Films. *Opt. Mater. Express* **2016**, *6* (11), 3622.

(52) Ciesielski, A.; Skowronski, L.; Trzcinski, M.; Szoplik, T. Controlling the Optical Parameters of Self-Assembled Silver Films with Wetting Layers and Annealing. *Appl. Surf. Sci.* **2017**, *421*, 349–356.

(53) Gubaydullin, A. R.; Symonds, C.; Bellessa, J.; Ivanov, K. A.; Kolykhalova, E. D.; Sasin, M. E.; Lemaitre, A.; Senellart, P.; Pozina, G.; Kaliteevski, M. A. Enhancement of Spontaneous Emission in Tamm Plasmon Structures. *Sci. Rep.* **2017**, *7* (1), 9014.

(54) Feng, S.-W. Dependence of the Dynamics of Exciton Transport, Energy Relaxation, and Localization on Dopant Concentration in Disordered C545T-Doped Alq_3 Organic Semiconductors. *Opt. Mater. Express* **2014**, *4* (4), 798.

(55) Liu, B.; Wu, R.; Menon, V. M. Propagating Hybrid Tamm Exciton Polaritons in Organic Microcavity. *J. Phys. Chem. C* **2019**, *123* (43), 26509–26515.

(56) Coropceanu, V.; Chen, X.-K.; Wang, T.; Zheng, Z.; Brédas, J.-L. Charge-Transfer Electronic States in Organic Solar Cells. *Nat. Rev. Mater.* **2019**, *4* (11), 689–707.

(57) Ghosh, S. K.; Pal, A.; Kundu, S.; Nath, S.; Pal, T. Fluorescence Quenching of 1-Methylaminopyrene near Gold Nanoparticles: Size Regime Dependence of the Small Metallic Particles. *Chem. Phys. Lett.* **2004**, *395* (4–6), 366–372.

(58) Sun, G.; Khurgin, J. B.; Soref, R. A. Plasmonic Light-Emission Enhancement with Isolated Metal Nanoparticles and Their Coupled Arrays. *J. Opt. Soc. Am. B* **2008**, *25* (10), 1748.

(59) Konrad, A.; Metzger, M.; Kern, A. M.; Brecht, M.; Meixner, A. J. Revealing the Radiative and Non-Radiative Relaxation Rates of the Fluorescent Dye Atto488 in a λ/2 Fabry–Pérot-Resonator by Spectral and Time Resolved Measurements. *Nanoscale* **2016**, *8* (30), 14541–14547.

(60) Marian, C. M. Spin-Orbit Coupling and Intersystem Crossing in Molecules. *WIREs Comput Mol Sci* **2011**, *2* (2), 187–203.

(61) Giebink, N. C.; Sun, Y.; Forrest, S. R. Transient Analysis of Triplet Exciton Dynamics in Amorphous Organic Semiconductor Thin Films. *Organic Electronics* **2006**, *7* (5), 375–386.

(62) Laussy, F. P.; del Valle, E.; Tejedor, C. Luminescence Spectra of Quantum Dots in Microcavities. I. Bosons. *Phys. Rev. B* **2009**, *79* (23), 235325.

Graphical TOC Entry

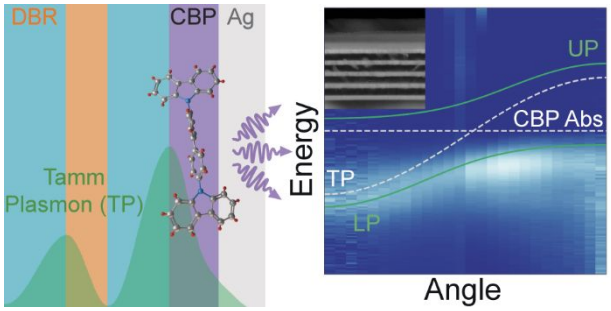

TOC Graphic. Graphic illustrating strong coupling in the Tamm plasmon cavity filled with CBP molecules and the results of angle-resolved PL measurements.

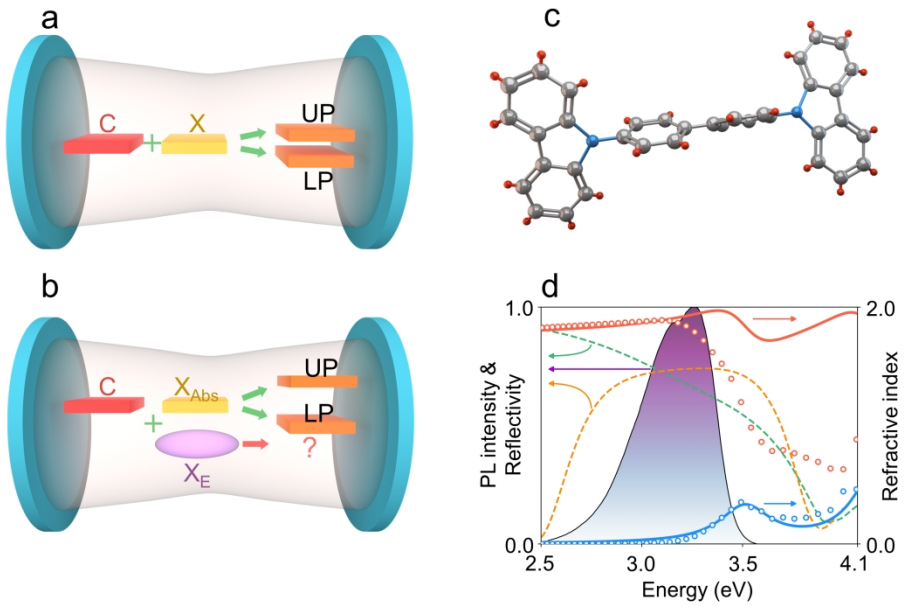

Figure 1. Sketch of the strong coupling regime phenomenon in the inorganic semiconductor cavities case (a) and in the organic cavity (b). (c) Molecular structure of the CBP material. (d) Left axis: CBP PL spectrum (black curve with a purple fill), calculated silver mirror reflectivity spectrum (green dashed curve) and DBR reflectivity spectrum (orange dashed curve) at normal incidence. Right axis: Contribution of experimental real (red circles) and imaginary (blue circles) parts of CBP refractive index. Solid red and blue lines show an approximation of the refractive indexes real and imaginary parts using expression (1).

254x153mm (300 x 300 DPI)

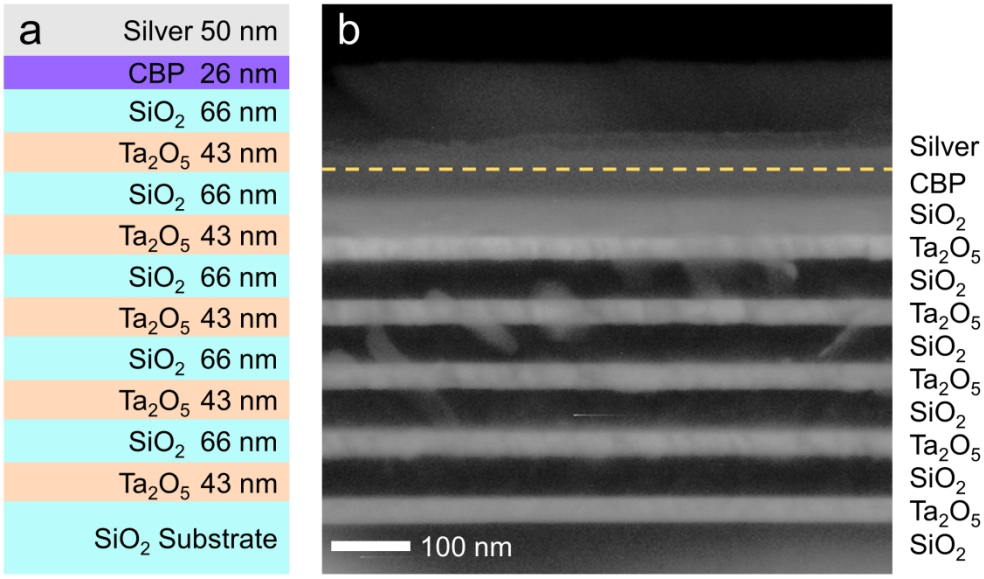

Figure 2. (a) Scheme of Tamm structure under study. (b) SEM image of the structure.

228x135mm (300 x 300 DPI)

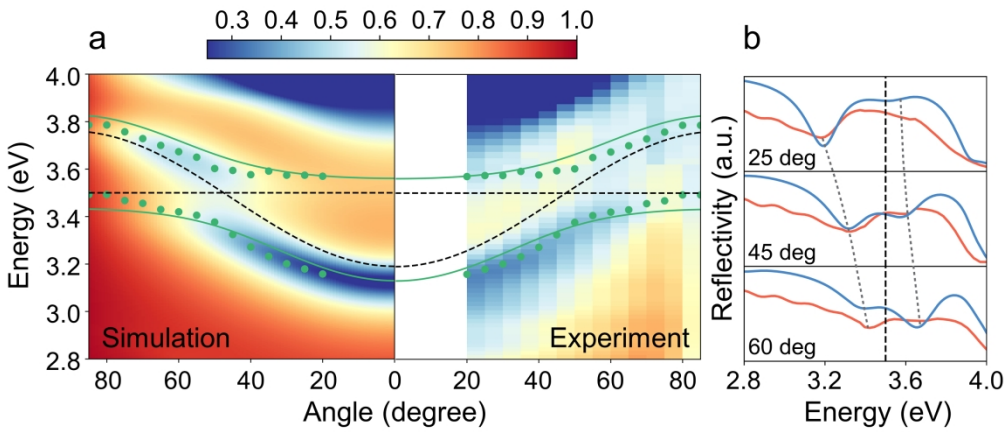

Figure 3. (a) Left part: Calculated reflectivity of TP/CBP structure as a function of the incidence angle and energy for TE – polarization case. Dashed black curves demonstrate dispersion of the neat Tamm plasmon state and the CBP exciton. Right part: Measured reflectivity of TP/CBP structure as a function of the incidence angle and energy. Green circles with error bars show the fitting results of the measured reflectivity spectra. Solid green curves show dispersions of the LP and UP branches obtained by eq. (2). (b) Measured (red curve) and calculated (blue curve) reflectivity spectra of the TP/CBP structure for the set of angles (25 degrees, 45 degrees, 60 degrees). Dashed black curve demonstrate the CBP exciton energy, dashed grey curves shows the positions of the upper and lower polariton branches.

254x110mm (300 x 300 DPI)

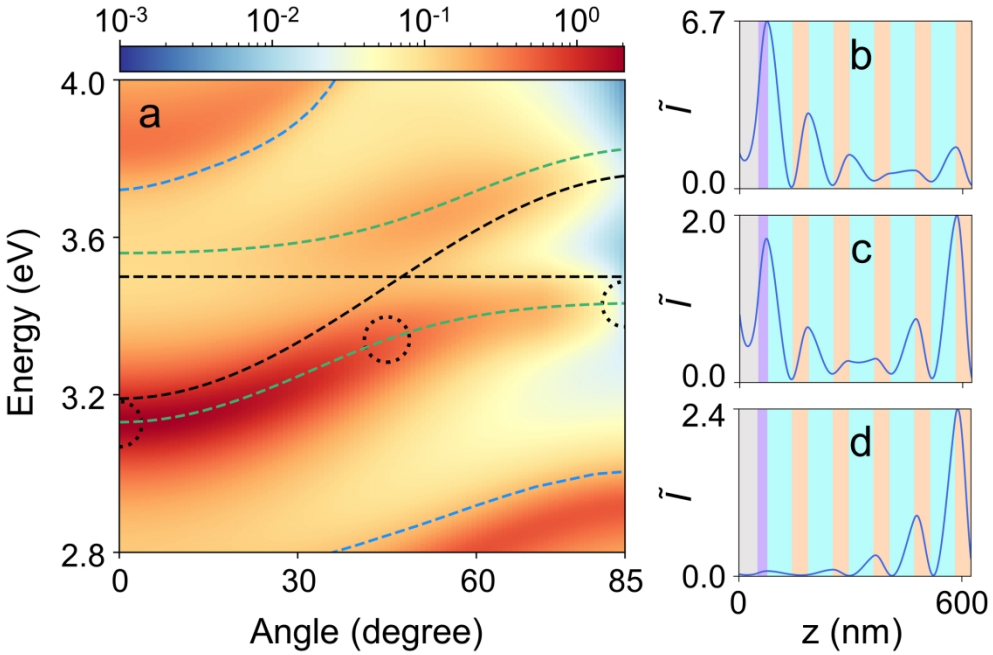

Figure 4. (a) dependence of the modal Purcell factor on the energy and angle of the Tamm plasmon structure for the emitter placed in the centre of the CBP layer. Dashed green curves show dispersions of the LP and UP branches obtained by eq. (2). Dashed black curves demonstrate the dispersion of the bare Tamm plasmon state and the CBP exciton. Dashed blue curves show the edges of the PBG. On the right side: Spatial profiles of the electric field squared I(z) along the LP branch for angle θ = 0 degrees; 45 degrees, and 85 degrees as marked by circles in figure 4a.

199x134mm (300 x 300 DPI)

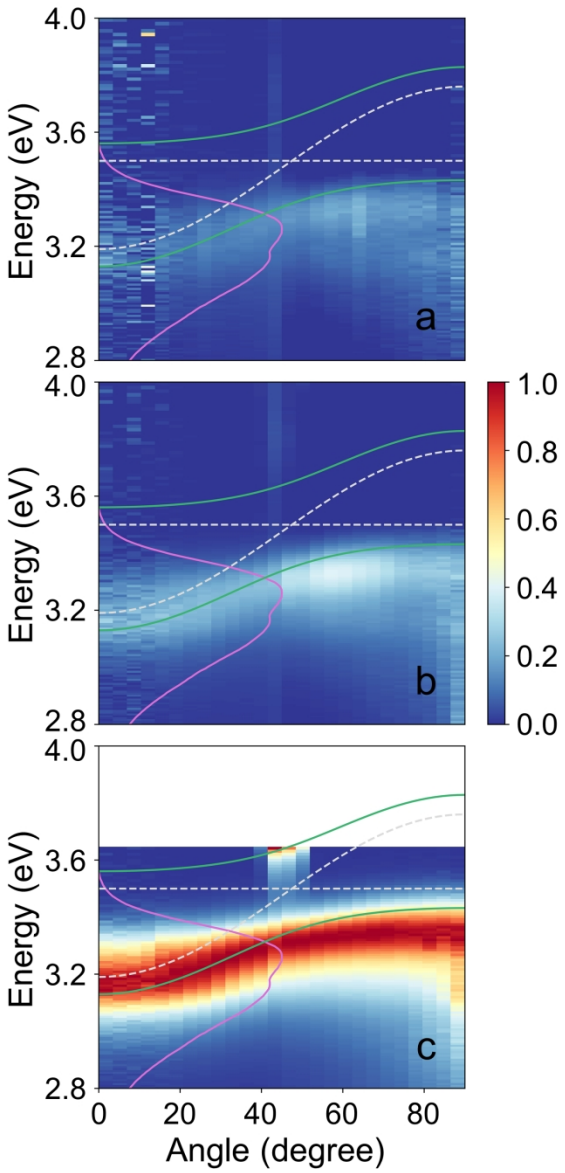

Figure 5. Results of steady-state PL measurements of the TP/CBP structure at various emission angles for a set of different excitation energies: 4.76 eV(a), 4.27 eV (b) and 3.75 eV (c) normalized at maximum intensity in all cases. Purple curves show the PL spectrum of the neat CBP. Dashed grey curves demonstrate dispersion of the neat TP state and the CBP exciton. Solid green curves show dispersions of the LP and UP branches obtained by eq. (2).

122x254mm (300 x 300 DPI)

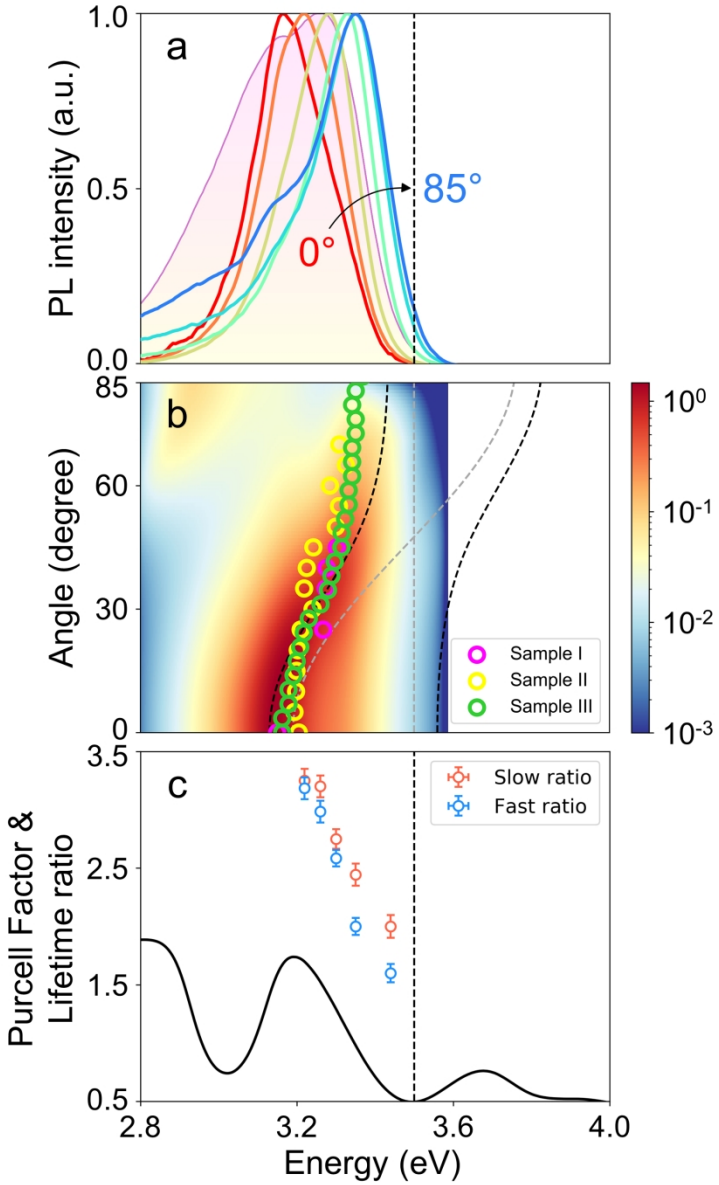

Figure 6. (a) the PL spectra of the TP/CBP structure for different emission angles: from 0 degrees (red curve) to 85 degrees (blue curve). The filled solid purple curve on the background shows the PL spectrum of the bare CBP. (b) Product of the modal Purcell factor and the CBP emission spectra. Open circles show the positions of the PL peak maxima of the LP emission for different samples. Dashed grey curve demonstrates the dispersion of the TP state. Dashed black curves shows the dispersion of the lower (LP) and upper polariton (UP) branches. (c) Calculated integral Purcell factor (solid black line) for a dipole placed in the centre of the TP/CBP structure. Open blue and red circles with error bars show the ratios for the fast ($\tau_{CBP}^{(1)}/\tau_{LP}^{(1)}$) and for the slow ($\tau_{CBP}^{(2)}/\tau_{LP}^{(2)}$) decay regions (see Figure 6). The dashed vertical curve on all figures demonstrates the CBP exciton energy.

154x254mm (300 x 300 DPI)

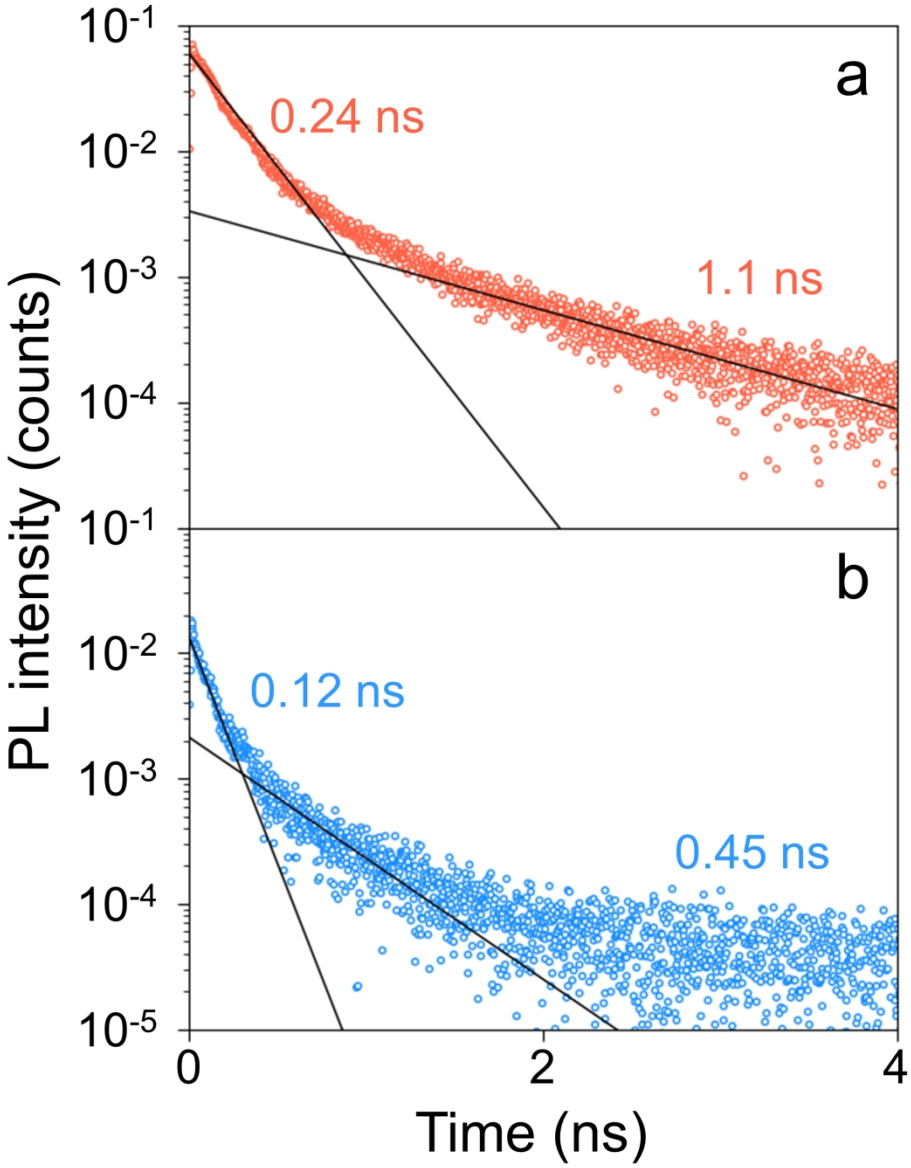

Figure 7. Decay of the PL intensity from neat CBP layer (a) and from the Tamm plasmon/CBP structure (b) for the energy 3.35 eV.

178x210mm (300 x 300 DPI)